SAND2015-1683C

9th U. S. National Combustion Meeting
Organized by the Central States Section of the Combustion Institute
May 17-20, 2015
Cincinnati, Ohio

Study of the momentum coupling between liquid fuel and ambient gas during injection using a dense spray formulation

F. Doisneau[1,⋆], M. Arienti[1], J. C. Oefelein[1]

[1]Combustion Research Facility, Sandia National Laboratories, Livermore CA 94551-0969, USA
⋆Corresponding Author Email: fdoisne@sandia.gov

Abstract: We study the momentum coupling between a liquid phase injected at high speed and a quiescent gas using a dense spray parallel code architecture and LES. The architecture is designed to handle strong loadings of liquid in an efficient, accurate, and robust way. It has the potential to handle important features of atomization and dense spray phenomena. As a first step, we focus on the way the dense liquid jet entrains the gas, creates turbulence, and is dispersed by it. This is an essential element to predict the fuel evaporation and mixing topology. We focus on a progression of studies to demonstrate the potential merits of the model and assess requirements for systematic incorporation and validation of key spray phenomena with emphasis placed on fuel injection processes in advanced internal-combustion engines.
Keywords: Dense multiphase flow, Spray evaporation, LES, Fuel injection

1. Introduction

Multiphase combustion processes are prevalent in many advanced combustion systems, e.g., internal combustion engines and gas turbines for propulsion and power. Treating these processes involves the variety of challenges associated with turbulence in the gas phase system, plus significant additional complications that arise due to the presence of multiple phases. Multi-scale coupling between processes occurs over a wide range of time and length scales, many being smaller than can be resolved in a numerically feasible manner. Further complications arise when liquid phases are present due to the dynamically evolving interface boundaries and the complex exchange processes that occur as a consequence. At the device level, high-performance, dynamic stability, low pollutant emissions, and low soot formation must be achieved simultaneously in complex geometries that generate complex flow and acoustic patterns. Flow and combustion processes are highly turbulent; i.e., integral-scale Reynolds numbers of $O(10^5)$ or greater, and the turbulence dynamics are inherently dominated by geometry or various operating transients. In modern systems, operating pressures now approach or exceed the thermodynamic critical pressures of the working fluids. Operation at elevated pressures introduces significant thermodynamic non-idealities and transport anomalies in low-temperature regions. Elevated pressures also significantly increase the system Reynolds number(s), which inherently broadens the range of spatial and temporal scales that interactions occur over.

The current study aims at developing a model that treats the complex processes associated with dense sprays and atomization. The model is developed explicitly for use with the Large Eddy Simulation (LES) technique. Recognizing the strong density differences between the high-speed liquid and the high-pressure chamber gas, it is crucial for the model and its associated numerical method to be able to describe the sharp interfaces that occur in both the (subcritical) case of discontinuities

that are resolved within a few molecular lengths, or in the (supercritical) case of real-fluid thermophysical property gradients. The merits of using kinetic theory are investigated as a comprehensive and flexible model framework for treating a disperse phase, either of spherical droplets, oscillating liquid blobs, or dense fluid regions with a diffuse interface. The approach relies on two separate systems of equations for the multicomponent gas and the dense fluid, following past examples [1, 2]. We devise a set of numerical methods including a transport scheme to maintain the sharp fronts of density without explicitly tracking the interface, and an operator splitting approximation that is tailored to enforce tight coupling between the two numerical phases. The approach is tested for its ability to reproduce the dynamics of the mixture's momentum (and therefore momentum coupling) during the initial stages of injection when the dense liquid core penetrates the chamber and strongly entrains the surrounding gas. In Section 2, we introduce the fluid-kinetic model framework and a reduction technique that leads to the baseline set of governing equations. In Section 3, the approach is partially validated using cases that are representative of realistic injection conditions. At the early stage of injection, results are compared to those obtained with an interface tracking method. At a later stage of the injection transient, the model's ability to render a detailed level of induced turbulence is analyzed. The study concludes on the potential of the model to achieve affordable yet high-fidelity LES of injection through the simulation of two-way coupled fluids.

2. An approach based on kinetic theory for LES of liquid injection processes

Alternative methods for treating the multiphase mechanisms of liquid injection focus on tracking the complex, corrugated, gas-liquid interface [3, 4, 5, 6]. For convenience, we refer to this approach as DNS. While potentially accurate, these methods can impose a prohibitive cost for full engine simulations. Mesoscopic models, as opposed to a microscopic description of the interface length scale, offer an affordable alternative provided that a satisfactory filtering procedure (e.g., ensemble averaging, time/space filtering) and the corresponding closures are established. To-date, the application of mesoscopic modeling of liquid fuel injection processes has been done using two very different approaches:

1. Extending classical theory of dilute sprays [1, 7, 8] by assuming thermodynamic stability at the sharp interface between liquid and gas and then modeling the sub-grid effects by assuming a prescribed topology; e.g., drops [9, 10, 11].
2. Accounting for the imbalance of the gas-liquid interfacial transport by bundling all the components and phases into a single comprehensive (non-ideal) thermodynamics [12] leads to real-gas simulation [13].

The first approach splits the numerical difficulty of transporting the liquid and gas disparate phases and offers a wide variety of possible closures. The second approach is promising for its consistency in treating real-fluid thermodynamics and transport but raises numerical complications in handling the gradients associated with the non-linearities of non-ideal thermodynamics. Here we aim to combine the approaches by considering both the problems and opportunities. By developing well suited numerical methods for a multi-fluid description, we aim at mitigating the issue of thermodynamic stiffness and open the path for a systematic modeling effort that takes advantage of the closure flexibility. The model is designed to emulate the following stages of injection. The first is the inertial behavior of the dense liquid core (or ballistic behavior). The second is the dispersion of liquid blobs (requiring a prescription of these structures' topologies). The third is the dilute spray regime.

In the following, we analyze the ability of such a model to describe the momentum coupling between the injected liquid and the chamber gas, keeping in mind that in the absence of further modeling, this approach cannot directly render either the way turbulence and surface tension affect the propagation of the liquid core, or the formation and exact spreading of the droplets.

2.1. Two-way coupled multi-fluid description

The model is based on the statistical approach for a spray [1], which can describe any disperse liquid structures suspended in a carrier gas. It results in a fluid-kinetic model and a set of continuous fluid equations for the gas, e.g. Navier-Stokes, that are strongly coupled to a statistical equation for the disperse phase. The coupling is achieved through momentum source terms accounting for drag in a conservative way. Heat and mass transfer are not considered for the sake of simplicity but the methodology is intended to be straightforward extended to these terms. This description can be easily closed if the liquid structures are spherical enough [14], which is presumably not the case during primary atomization with the presence of the dense liquid core. But resorting to spray closures; i.e., tracking only one size parameter for the liquid and using drop correlations as closures, is a first step to a more detailed description. The disperse phase is accounted for by a Number Density Function (NDF), $f(t, \boldsymbol{x}; \boldsymbol{c}, r)$, where velocity $\boldsymbol{c}$ and radius r are the only information available from the microscopic liquid structure level. The NDF is governed by the kinetic equation [1]:

$$\partial_t f + \partial_{\boldsymbol{x}} \boldsymbol{c} f + \partial_{\boldsymbol{c}} \boldsymbol{F} f = 0 \tag{1}$$

where $\boldsymbol{F}$ is the drag force and depends on the local gas and drop velocity, gas viscosity μ_g, and drop size r. Stokes' law for spheres is chosen as a simplified closure, with a characteristic time $\tau^{\boldsymbol{u}} = 2\rho_l r^2/(9\mu_g)$. In this equation, mass transfer (evaporation), thermal transfer, collisions, and break-up are not accounted for, which is consistent with our current goals of focusing only on momentum coupling.

The NDF has a high dimensional phase space (4D in addition to the 4D of space and time) so it is reduced by assuming a particular shape [2]:

$$f(t, \boldsymbol{x}; \boldsymbol{c}, \theta, r) \approx \tilde{f}(t, \boldsymbol{x}; \boldsymbol{c}, \theta, r) = \sum_{k=1}^{N_{\text{sec}}} \kappa_k(t, \boldsymbol{x}; r) \delta(\boldsymbol{c} - \boldsymbol{u}_k(t, \boldsymbol{x})) \tag{2}$$

with κ_k a family of size presumed PDFs that are zero outside of the section intervals $[r_{k-1}, r_k]$. Reducing the velocity distribution to a Dirac δ-function and parameterizing the velocity moment with the section index k embodies the assumption of size-conditioned velocities. This presumed shape is valid as long as r is below a flow-dependent critical size [14], above which trajectory crossings would occur in vortical and stretched zones. With this approximation, referred to as multi-fluid in the following, any NDF in the phase space can be uniquely reconstructed from the knowledge of a set of moments in size and velocity:

$$\begin{pmatrix} m_{k,0} \\ \dots \\ m_{k,n} \\ m_{k,3}\boldsymbol{u}_k \end{pmatrix} (t, \boldsymbol{x}) = \int_{r_{k-1}}^{r_k} \int_{\mathbb{R}^+} \int_{\mathbb{R}^{\sharp}} \begin{pmatrix} 1 \\ \dots \\ r^n \\ r^3\boldsymbol{c} \\ r^3\theta \end{pmatrix} \tilde{f}(t, \boldsymbol{x}; \boldsymbol{c}, r) \mathrm{d}\boldsymbol{c}\mathrm{d}r, \qquad k \in [\![1; N_{\text{sec}}]\!] \tag{3}$$

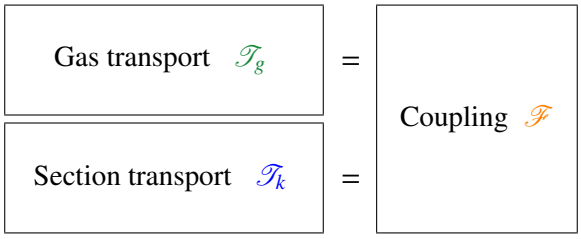

Figure 1: Illustration of the present splitting strategy.

where the number of size moments n is related to the number of unknown parameters in the presumed shapes κ_k. This equivalence holds as long as $r_0 < r_1 < ... < r_{N_{\text{sec}}} = +\infty$ is a partition of the size phase space. The N_{sec} intervals are referred to as the sections [2]. In the following, we consider two moments in size per section that is mass, simply noted as

$$\begin{pmatrix} m_{k,0} \\ m_{k,3} \end{pmatrix} = \begin{pmatrix} n_k \\ m_k \end{pmatrix},$$

so that we need to account for four moments per section. The disperse phase is described by $6N_{\text{sec}}$ scalar Eulerian fields in 4D, instead of a scalar 9D problem. For the fully coupled problem, the governing equations finally read:

$$\left\{ \begin{array}{lcl} \partial_t \rho_g + \partial_{\boldsymbol{x}} \rho_g \boldsymbol{u}_g & = & 0 \\ \partial_t \rho_g \boldsymbol{u}_g + \partial_{\boldsymbol{x}} \rho_g \boldsymbol{u}_g \otimes \boldsymbol{u}_g & = & -\partial_{\boldsymbol{x}} p - \displaystyle\sum_k \boldsymbol{F}_k \\ \partial_t \rho_g e_g + \partial_{\boldsymbol{x}} \rho_g e_g \boldsymbol{u}_g & = & -p \partial_{\boldsymbol{x}} \boldsymbol{u}_g + \displaystyle\sum_k \boldsymbol{F}_k (\boldsymbol{u}_g - \boldsymbol{u}_k) \\ \partial_t n_k + \partial_{\boldsymbol{x}} n_k \boldsymbol{u}_k & = & 0 \\ \partial_t m_k + \partial_{\boldsymbol{x}} m_k \boldsymbol{u}_k & = & 0 \\ \partial_t m_k \boldsymbol{u}_k + \partial_{\boldsymbol{x}} m_k \boldsymbol{u}_k \otimes \boldsymbol{u}_k & = & \boldsymbol{F}_k \end{array} \right\} \quad k \in [\![1; N_{\text{sec}}]\!] \tag{4}$$

This is referred to as the Dense Multi-Fluid model in the following.

2.2. *Time integration of the coupled system*

The choice of splitting Eq. (4) allows one to use time integration schemes that are dedicated to the peculiarities of its different parts. The couplings can be rendered accurately if the operators and splitting sequence are defined correctly, and if the overall splitting time-step Δt is well chosen. A more complete discussion on splitting, as applied to coupled spray systems, can be found in [15]. In the present, we define the three operators illustrated in Figure 1. These are the gas transport $\mathscr{T}_g$, section transport $\mathscr{T}_k$, where $k \in [\![1; N_{\text{sec}}]\!]$, and the relaxation operator $\mathscr{F}$ that describes how fast the liquid and gas velocities converge locally to an equilibrium value in a way that conserves the system's momentum.

The transport part of the gas phase, $\mathscr{T}_g$, reduces to the Navier-Stokes equation, for which a staggered explicit time integration method (RK4) with 3rd order fluxes is chosen [16]. This allows one to account accurately for both the convective and acoustics structures in the flow and requires, for high Reynolds numbers, to observe the CFL constraint

$$\tau_g < \min\left(\frac{\Delta x}{|\boldsymbol{u}_g| + c}\right). \tag{5}$$

The coupling operator, $\mathscr{F}$, is a set of ODEs

$$\begin{cases} \mathrm{d}_t \rho_g \boldsymbol{u}_g = -\sum_k \boldsymbol{F}_k \\ \mathrm{d}_t m_k \boldsymbol{u}_k = \boldsymbol{F}_k \qquad\qquad k \in [\![1; N_{\mathrm{sec}}]\!] \end{cases} \tag{6}$$

that can be integrated explicitly provided that the time scales of the drag for the two-way coupled system are larger than the overall splitting time-step Δt. Note that the characteristic time for drag for the two-way coupled system gets shorter with a higher liquid loading. This time is locally of the order

$$\tau_c = \min_k \left(\frac{\tau^{\boldsymbol{u}}(r_k)}{1 + m_k/\rho_g} \right). \tag{7}$$

As a consequence, the discrepancies introduced by spherical closures on momentum coupling do not have a significant impact in the regions where the dynamics is dominated by the liquid and the velocities just need to be maintained close to equilibrium. To respect the coupling between the dense phase and gas phase, the splitting time-step is chosen to be equal to the gas phase time-step following a standard CFL constraint. Finally, the transported part of the disperse phase, $\mathscr{T}_k$, reduces to N_{sec} systems:

$$\begin{cases} \partial_t n_k + \partial_{\boldsymbol{x}} n_k \boldsymbol{u}_k = 0 \\ \partial_t m_k + \partial_{\boldsymbol{x}} m_k \boldsymbol{u}_k = 0 \\ \partial_t m_k \boldsymbol{u}_k + \partial_{\boldsymbol{x}} m_k \boldsymbol{u}_k \otimes \boldsymbol{u}_k = 0 \end{cases} \tag{8}$$

with a behavior equivalent to so-called pressureless gas dynamics [17].

2.3. Semi-Lagrangian scheme: a gather-scatter sequence

To solve Eq. (8), we resort to a numerical algorithm that benefits from the system's pressureless nature. The trajectories are assumed to never influence each other, except in case of crossings, so that transport can be efficiently described with Lagrangian particles. For this, we introduce the following sequence as a resolution approach for $\mathscr{T}_k$:

1a) Scatter: Given Eulerian fields at time t, parcels are defined with positions that match the nodes. At a given node, as many parcels can be defined as needed to describe the Eulerian information with the desired accuracy (i.e., multiple but discrete velocities to render crossings or dispersion, and multiple discrete or continuous sizes, temperatures, and shapes *etc.*). The mapping from an Eulerian description to a Lagrangian (mesh-less) description at time t reads:

$$\begin{pmatrix} n_k \\ m_k \\ m_k \boldsymbol{u}_k \end{pmatrix} (t, \boldsymbol{x}) \text{ with } k \in [\![1; N_{\mathrm{sec}}]\!] \rightarrow \begin{pmatrix} \boldsymbol{x}_p \\ n_p \\ m_p \\ \boldsymbol{u}_p \end{pmatrix} \text{ with } p \in [\![1; N_p]\!], \tag{9}$$

where $\boldsymbol{x}_p(t) = \boldsymbol{x}$ and $m_p(t) = m_k \mathcal{V}_{\mathrm{node}}$. In the multi-fluid context, we also have $N_p = N_{\mathrm{sec}}$ since the assumption of size conditioning has allowed us to resort to one parcel per section in order to achieve one parcel per velocity.

1b) Transport: All the Lagrangian parcels are advected at their own velocity on Δt. The characteristics of Eq. (8) are straight lines so that this step is a trivial linear extrapolation, being exact in the splitting context.

2a) Gather: A projection technique (detailed in Appendix A) is used to gather the Lagrangian information at $t + \Delta t$ (now at arbitrary locations, which do not match the Eulerian grid) towards fixed Eulerian nodes. This projection is linear with respect to mass but will induce an overall non-linearity in the case where velocities are averaged at the nodes. An illustration of this fact is that the trajectories of two jets crossing each other is not solved as the superposition of each of the two jet trajectories [14]. Instead the jet momenta are averaged and relative kinetic energy is dissipated as if perfectly inelastic collisions occurred. At this point, the Eulerian field is the solution of Eq. (8) at time $t + \Delta t$ and the transport step is finished.

2b) Phase Space Evolution: In the context of the above splitting, the rest of Eq. (4) should be solved. The Eulerian fields encounter a phase space evolution (here reduced to drag $\mathscr{F}$) on Δt. At the end of this step, the Eulerian field is the approximated solution of System (4) at time $t + \Delta t$. This splitting is a first order Lie splitting [18].

Step 1a) can be renewed, defining the Lagrangian state at $t + \Delta t$. So the splitting sequence can be summarized using symbolic operator notations as follows:

$$\boldsymbol{U}(t+\Delta t) = \mathscr{R} \prod_{k=1}^{N_{\text{sec}}} (\mathscr{T}_k)\ \mathscr{T}_g\ \boldsymbol{U}(t) \quad \text{with} \quad \boldsymbol{U}(t) = \begin{pmatrix} \rho_g \\ \rho_g \boldsymbol{u}_g \\ \rho_g e_g \\ n_k \\ m_k \\ m_k \boldsymbol{u}_k \end{pmatrix} (t).$$

The key is to perform frequent projections of the mass and momentum on an Eulerian mesh in order to use the Eulerian fields for the coupling step (Euler-Euler coupling), and redefine the way the field is sampled by Lagrangian parcels (Lagrangian remeshing). These two steps of the Eulerian projection contribute to both increasing the overall accuracy and parallel efficiency.

3. Results in Spray A conditions

The model and methodology outlined above have been implemented in the RAPTOR code developed by Oefelein [16]. We consider conditions from the ECN (Engine Combustion Network) Spray A case [19]. Here n-dodecane ($\rho_l = 702\,\text{kg/m}^3$) is injected at sonic speed ($\boldsymbol{u}_k(t, \boldsymbol{x}_0) = 600\,\text{m/s}$) by a single injector ($d_{in} = 90\,\mu\text{m}$) into a hot pressurized chamber ($T_g = 900\,\text{K}$, $P_g = 60\,\text{bar}$, $\rho_g = 22.8\,\text{kg/m}^3$). At present, the nozzle flow is not computed. Instead a laminar plug-flow profile is used, which is responsible for a significant discrepancy with experimental spray angles but does not interfere with the present code-to-code comparisons. The geometry is simplified to a box of dimensions $9600 \times 3200 \times 3200\,\mu\text{m}^3$ discretized as a cartesian mesh of $768 \times 256 \times 256$ cells, which translates to 7 cells per nozzle diameter.

To perform the study of momentum coupling, no heating or evaporation is considered for the sake of simplicity. For the drag force characteristic time, the equivalent drop radius is taken to be $r = 2\,\mu\text{m}$, which leads to coupling times that are close to and above the computation time-step. The latter is constrained by the Navier-Stokes solver CFL time, τ_g, which is approximately $\Delta t = 8\,\text{ns}$. The impact of this choice for the characteristic coupling time is discussed below.

3.1. Computational efficiency

From a computational efficiency perspective, the Dense Multi-Fluid simulations are run on 576 cores with a characteristic computational time that is less than twice that of the Navier-Stokes solver. This provides a good indicator of the scalability of the method given that the required time-step is the one that would prevail with the sole (Navier-Stokes) CFL condition. In the present Eulerian approach for the liquid phase, the number of degrees of freedom is fixed by the size of the mesh. This fixed spatial discretization has two consequences:

- the accuracy does not depend on a user-defined sampling, or on the way the samples are transported, and is the same in both the dense and dilute regions;
- the computational load is more easily forecast, being fixed wherever there is mass and the solver being turned off in vacuum regions.

The new method is deterministic and therefore does not require extra efforts on noise control or post-processing, assuming that we are ultimately interested in Eulerian fields. All these qualities are promising for the present application, for larger computations such as reactive ones, and for mechanical engineering applications in general.

3.2. Early injection stage

To provide a comparison between methods and approaches, a set of calculations have been performed using both the Dense Multi-Fluid model describe here, and the Coupled Level-Set Volume of Fluid (CLSVOF) approach [20]. The CLSVOF approach is a state-of-the-art interface-capturing method which we expect to provide a reference on momentum coupling between liquid and gas: it accounts for the sharp interface allowing the conservation of volume and the accurate computation of the surface tension. The comparison is conducted at an early stage of injection, namely when the liquid trajectory is weakly influenced by the surrounding gas. We choose to look at the instant $3.7\,\mu$s after the start of injection (ASI) with the model boundary condition described above for the liquid. Results are given in Figure 2. Strong entrainment is created in the chamber because the liquid mass fraction and momentum ratio are high. The two approaches agree very well on the gas flow field and on the inertial behavior of the liquid core but the penetration is 10% overestimated by the Dense Multi-Fluid approach. Also, the tip of the jet has a more elongated shape presumably due to the lack of surface tension.

3.3. Late injection stage

The Dense Multi-Fluid injection calculation described above was analyzed at a further time to assess the nature of the flow that is generated as a consequence of liquid entrainment. Results are presented in Figure 3, which shows that the liquid has been dispersed and the gas perturbed. A part of the intact liquid core penetrates and crosses the domain, but a significant amount of liquid is also dispersed within a cross sectional area that is approximately 10 times wider than the nozzle diameter. This spread liquid features strong non-uniformities of mass concentration (we emphasize that the scale is logarithmic), as a result of the inertial transport in the turbulent gas flow. At the chosen instant, the spreading of the liquid does not increase with axial distance, and therefore does not reproduce the cone-shape of typical sprays. This difference presumably stems from two facts:

- the boundary condition is unphysical and introduces a cylinder-shaped liquid,

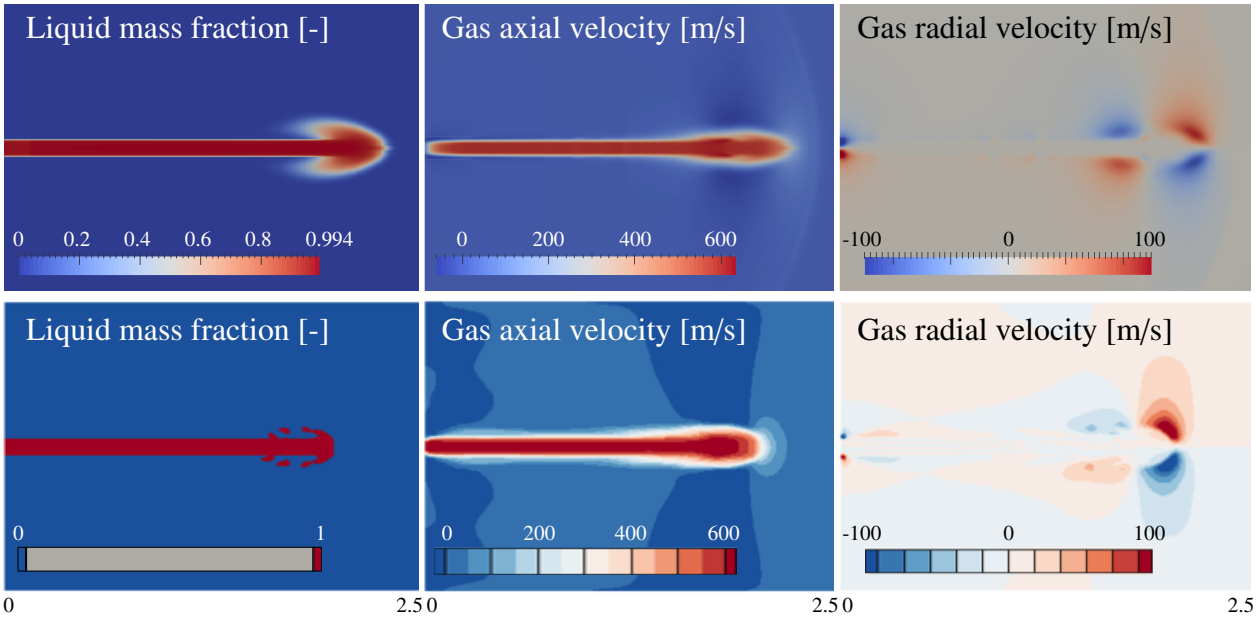

Figure 2: Dense Multi-Fluid (top) and CLSVOF (bottom) injection with a laminar boundary condition at 3.7 μs ASI (center plane slices) – Lengths are in mm.

- the chosen profile does not reflect the level of initial perturbations that exist in actual injectors, where strong turbulence and sometimes cavitation are produced within the nozzle and the internal Reynolds number is of order of 10^5.

In the gas phase, the axial velocity reaches the liquid velocity in the region where the liquid mass fraction is close to 1. At the edge of the dense liquid region, the outer fluid reacts to shear in a manner similar to that produced by a material interface (solid wall). The position of the shear layer is known less accurately (within Δx) for the Dense Multi-Fluid method. The choice of the coupling time (based on an equivalent drop size) has no influence as long as the loading is high since we are dealing with a liquid-gas flow that relaxes towards equilibrium faster than the other time scales of the flow. The simulation produces a large amount of turbulence in the chamber. The maximum levels are half of $\boldsymbol{u}_k(t, \boldsymbol{x}_0)$ for the axial velocity, and one-sixth of it for the radial values. This induced turbulence is the result of a strong shear layer at the edge of the liquid core and it is responsible, together with the tearing away of the tip of the jet (see Figure 2), for the dispersion of the liquid that is observed in Figure 3.

4. Conclusion

To simulate fuel injection and mixing, we have assessed a new method based on the separate description of multiple fluids. The liquid model and solver are based on the kinetic approach for sprays, but dedicated numerical methods have been developed to handle the high loading and strong coupling that arise. A new physical-space transport method for high-loading sprays has shown that tight phase coupling can be achieved at a fraction of the cost of a multi-material method. This new approach possesses better convergence properties than a traditional Lagrangian parcel method. The degrees of freedom are attached to the mesh, which allows controlling accuracy and load balancing,

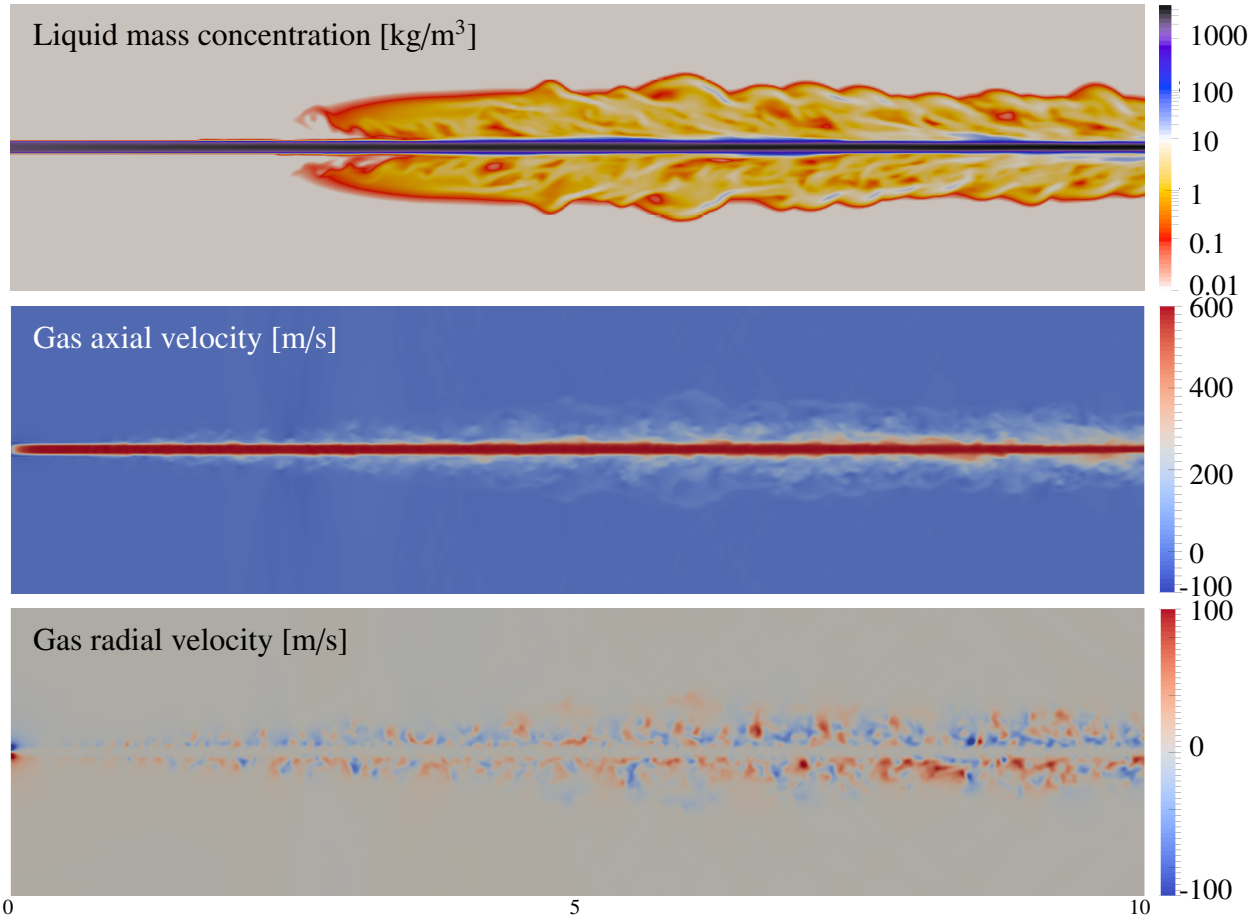

Figure 3: Dense Multi-Fluid injection with a laminar boundary condition at 30 μs after start of injection (center plane slices, lengths are in mm).

and avoids spurious interactions between the sampling choices and the physics. The new method is deterministic and therefore does not require extra efforts on noise control or post-processing. It also avoids flux computations in the physical space, which can be a stumbling block of Eulerian methods. All the couplings are done under the form of Eulerian fields, which is efficient for concurrent computing, as confirmed by early scaling tests. The robustness of this coupling strategy has allowed computing a supersonic injection of a highly loaded spray without any additional constraint than the CFL that applies to the gas phase solver. The first results suggest a promising alternative the DNS of two-phase flows, and give a detailed picture of the fine structures of the flow at a reasonable cost. In the prospect of a more detailed description including polydispersity, evaporation and combustion, the method's compatibility with the state-of-the-art descriptions for sprays is viable.

Appendix A. Projection technique

The novel aspect of the gather-scatter transport scheme presented in Section 2.3 is the ability to transform an instantaneous Lagrangian description (point-wise masses at arbitrary locations) into an Eulerian description (fixed locations). The projection technique used is described here. A

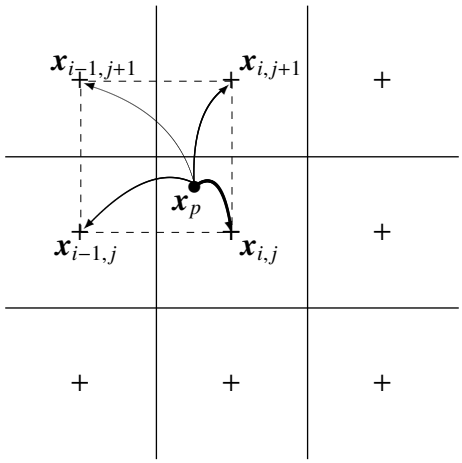

Figure A.4: Schematic of the projection step for particle p in a 2D cartesian mesh.

conservative projection is done on the 8 closest neighbors in 3D. The weights are based on the scalar distances of the parcel to the nodes, as shown in Figure A.4. An Eulerian node $\boldsymbol{x}_i$ receives mass from parcels

$$p \in \Omega_{\boldsymbol{x}_i} = \left\{ p \;\middle|\; \boldsymbol{x}_i - \begin{pmatrix} \Delta x^- \\ \Delta y^- \\ \Delta z^- \end{pmatrix} < \boldsymbol{x}_p < \boldsymbol{x}_i + \begin{pmatrix} \Delta x^+ \\ \Delta y^+ \\ \Delta z^+ \end{pmatrix} \right\}, \tag{A.1}$$

where $\Delta x^{\pm} = \mid x_{i,x} - x_{i\pm1,x} \mid$ so that parcels in immediately neighboring cells contribute to a cell as long as they are not beyond the center of the neighbors. The quantitative repartition is done using a weight function $w_{pi} = \prod_{\alpha \in x,y,z} w_{pi,\alpha}$ that, for isotropy reasons, is defined identically in each direction as:

$$w_{pi,x} = 1 - \eta_x, \quad w_{pi,y} = 1 - \eta_y, \quad w_{pi,z} = 1 - \eta_z. \tag{A.2}$$

The choice of $\eta_x = \frac{x_{p,x} - x_{i,x}}{x_{i\pm1,x} - x_{i,x}}$ is based on if $\boldsymbol{x}_p$ is closer to x_{i-1} or x_{i+1}. Mass conservation is then enforced as the seven other neighbors of p will receive contributions that are weighted by all the possibles products with the coefficients $w_{pi\pm1,x} = 1 - w_{pi,x}$, $w_{pi\pm1,y} = 1 - w_{pi,y}$, and $w_{pi\pm1,z} = 1 - w_{pi,z}$ that are complementary to one, thanks to the symmetry property. After gathering the conserved quantities from the old parcels within $\Omega_{\boldsymbol{x}_i}$, the following Lagrangian vector for the new parcel is obtained:

$$\begin{pmatrix} x_i \\ m_i = \displaystyle\sum_{p \in \Omega_{\boldsymbol{x}_i}} w_{pi} m_p \\ \phi_i = \dfrac{1}{m_i} \displaystyle\sum_{p \in \Omega_{\boldsymbol{x}_i}} w_{pi} m_p \phi_p \end{pmatrix}. \tag{A.3}$$

The old uncentered parcels are removed so that the spatial index is now $i \in [\![1, N_{\text{cell}}]\!]$, while the old index $p \in [\![1, N_s]\!]$ is no longer used. Recall that the sectional index k has been dropped but this operation must be performed separately for all the parcels of a section so that we now have exactly $N_{\text{sec}} \times N_{\text{cell}}$ parcels which can be again noted with the indices $(k, p = i)$.

References

[1] F. A. Williams, Physics of Fluids 1 (1958) 541–545.

[2] F. Laurent, M. Massot, Comb. Theory and Modelling 5 (2001) 537–572.

[3] T. Menard, S. Tanguy, A. Berlemont, International Journal of Multiphase Flow 33 (2007) 510–524.

[4] O. Desjardins, V. Moureau, H. Pitsch, Journal of Computational Physics 227 (2008) 8395–8416.

[5] M. Herrmann, Journal of Engineering for Gas Turbines and Power 132 (2010) 061506–10.

[6] M. Arienti, M. Sussman, International Journal of Multiphase Flow 59 (2014) 1–14.

[7] G. Faeth, Progress in Energy and Combustion Science 9 (1983) 1–76.

[8] R. Reitz, R. Diwakar, SAE PAPER 860469 (1986).

[9] S. Som, S. Aggarwal, Combustion and Flame 157 (2010) 1179–1193.

[10] J. Tillou, J.-B. Michel, C. Angelberger, D. Veynante, Combustion and Flame 161 (2014) 525–540.

[11] D. Kah, O. Emre, Q. Tran, S. Chaisemartin, S. Jay, F. Laurent, M. Massot, International Journal of Multiphase Flows 71 (2013) 38–65.

[12] R. Dahms, J. Oefelein, Physics of Fluids 25 (2013) 092103.

[13] G. Lacaze, A. Misdariis, A. Ruiz, J. Oefelein, Proceedings of the Combustion Institute (2014).

[14] S. de Chaisemartin, Polydisperse evaporating spray turbulent dispersion: Eulerian model and numerical simulation, Ph.D. thesis, Ecole Centrale Paris, 2009. Http://tel.archives-ouvertes.fr/tel-00443982/en/.

[15] F. Doisneau, A. Sibra, J. Dupays, A. Murrone, F. Laurent, M. Massot, Journal of Propulsion and Power 30 (2014) 727–747.

[16] J. C. Oefelein, Progress in Aerospace Sciences 42 (2006) 2–37.

[17] F. Bouchut, S. Jin, X. Li, SIAM J. Num. Anal. 41 (2003) 135–158.

[18] S. Descombes, M. Massot, Numer. Math. 97 (2004) 667–698.

[19] M. Bardi, R. Payri, L.-M. Malbec, G. Bruneaux, L. M. Pickett, J. Manin, T. Bazyn, C. Genzale, Atomization and Sprays 22 (2012).

[20] M. Jemison, M. Sussman, M. Arienti, Journal of Computational Physics 279 (2014) 182–217.